

Chapter 1

Common Tools and Techniques

1.1 Fourier Transform Spectroscopy

The radiance spectra used in both strands of this thesis were measured using Fourier transform spectrometers. The spectra are acquired by performing a Fourier transform to the output of an interferometer. The design of most interferometers is based on the two-beam Michelson interferometer (Michelson & Morley 1887), which is shown in figure 1.1, and the mathematical theory of the Michelson interferometer also applies in general to other designs of Fourier transform spectrometer. This section contains an explanation of the mathematical theory underlying the operation of an ideal Fourier Transform spectrometer and some further considerations that apply to the output of physical rather than ideal instruments, which is particularly relevant for the development of FINESSE described in chapter 2. This information is taken from textbooks written by Griffiths & de Haseth (1986) and Davis, Abrams & Brault (2001).

Figure 1.1 shows a schematic of a Michelson interferometer. Radiation that is incident on the aperture of the interferometer is collimated and then passed through a beam splitter. After this each beam of radiation is reflected by a mirror and then recombined at the same beamsplitter. One of the mirrors is movable such that the optical path difference between the two beams of light can be varied. The output is then incident on the detector where its intensity is measured. The intensity of the light at the output varies with the optical path difference introduced by the

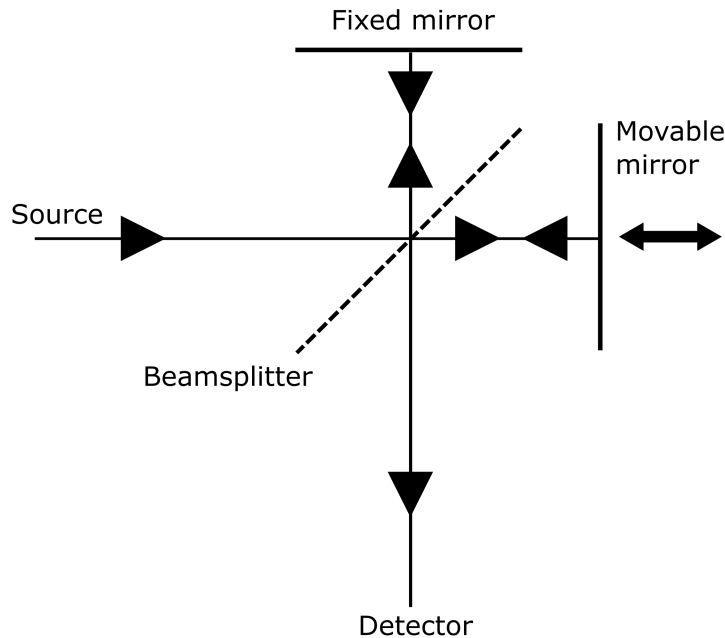


Figure 1.1: A schematic of a Michelson interferometer.

movable mirror. For monochromatic light the intensity at the detector will be at a maximum when the optical path difference is an integer multiple of the wavelength. If the mirror is scanned continuously, the signal at the detector will vary sinusoidally as a function of optical path difference. The signal measured at the detector is called the interferogram. Considering just the varying part of the signal and removing any DC offset gives the mathematical expression for the interferogram $I(\delta)$,

$$I(\delta) = B(\nu) \cos(2\pi\nu\delta) \quad (1.1)$$

where δ is the optical path difference, ν the wavenumber of the radiation and $B(\nu)$ is the intensity of the source radiation as modified by the characteristics of the instrument, including beam splitter efficiency and amplifier and detector response. This equation represents the Fourier transform of the input signal, modified by the instrument characteristics.

The same principle applies when a broadband source of radiation is incident on the spectrometer. In this case the energy detected is the sum of the energy detected for each frequency

making up the broadband source. Therefore the expression for the interferogram is

$$I(\delta) = \int_{-\infty}^{\infty} B(\nu) \cos(2\pi\nu\delta) d\nu. \quad (1.2)$$

The input spectrum (modulated by instrument characteristics) can then be retrieved using the FT pair of equation 1.2

$$B(\nu) = \int_{-\infty}^{\infty} I(\delta) \cos(2\pi\nu\delta) d\delta. \quad (1.3)$$

In theory a spectrum of arbitrarily high resolution could be produced by scanning an arbitrarily long optical path difference (OPD), however this is not possible in practice and the optical path difference has a maximum and minimum value of $\pm\Delta$ (assumed here to be symmetrical). To account for this, the theoretical arbitrarily wide interferogram is multiplied by a truncation function $D(\delta)$ such that

$$\begin{aligned} D(\delta) &= 1 && \text{if } -\Delta \leq \delta \leq \Delta, \\ D(\delta) &= 0 && \text{if } \delta > |\Delta|. \end{aligned} \quad (1.4)$$

$D(\delta)$ is commonly known as a boxcar function. The spectrum is recovered by performing a FT of the truncated interferogram

$$B(\nu) = \int_{-\infty}^{\infty} I(\delta) D(\Delta) \cos(2\pi\nu\delta) d\delta. \quad (1.5)$$

This has the effect of convolving the spectrum of arbitrary resolution with the function that is the FT of the boxcar, which is a sinc function of the form

$$f(\nu) = 2\Delta \operatorname{sinc}(2\pi\nu\delta). \quad (1.6)$$

This sinc curve has a height of 2Δ and a FWHM of $0.605/\Delta$ and is sometimes known as the “instrument line shape” (ILS) as it represents the response of the instrument to an infinitely

narrow spectral line represented by a delta function. Convolving the spectrum with a sinc function produces a large “ringing” effect in the spectrum around spectral lines that are narrow compared to the ILS, therefore extra processing can be done to remove these side lobes, at the expense of the loss of some spectral resolution. This is known as apodisation. Any function that has a value of 1 at $\delta = 0$ and that decreases to zero as $|\delta|$ increases can be used as an apodisation function. Some examples of common apodisation functions include triangles and gaussians, as well as functions designed explicitly for this purpose. The ILS is then the FT of this apodisation function multiplied by a boxcar of appropriate width.

Up to this point, we have assumed that the interferogram is symmetrical and can therefore be represented by the cosine Fourier transform. However, several processes can cause the interferogram to become asymmetrical. These include an error in location of the point of zero OPD or side effects of the electronic filters designed to reduce high frequency noise. These filters can put a wavenumber dependent phase lag on each cosine component of the interferogram, meaning that the point of zero path difference depends on the frequency of the radiation. The process of correcting for this phase lag and other phase errors to allow for the asymmetrical interferogram is known as phase correction. The phase lag or phase angle of the spectrum is usually a slowly varying function of frequency.

If interferogram is not symmetrical due to the phase angle, as is the case for real world measurements, we must use the complex FT to retrieve the complex spectrum $B'(\nu)$

$$B'(\nu) = \int_{-\infty}^{\infty} I(\delta) e^{-i2\pi\nu\delta} d\delta. \quad (1.7)$$

The complex spectrum $B'(\nu)$ contains all the spectral information of the source but the phase angle has dispersed some of this into the imaginary plane. The true spectrum $B(\nu)$, which is a real function without noise nonlinearities caused by phase angle, can be found from the complex spectrum using

$$B(\nu) = \text{Re}(\nu) \cos(\theta_\nu) + \text{Im}(\nu) \sin(\theta_\nu) \quad (1.8)$$

where $\text{Re}(\nu)$ and $\text{Im}(\nu)$ are the real and imaginary parts of the complex spectrum $B'(\nu)$, and θ_ν is the phase angle as a function of wavenumber. This correction assumes that the phase angle is a slowly varying function of wavenumber. The phase angle can be calculated using the Mertz method (Mertz 1965). In this method a truncated interferogram (usually of 128, 256 or 512 points) is collected around the centre burst of the interferogram. A FT is performed on this truncated interferogram, and the phase angle is calculated using

$$\theta_\nu = \arctan \left(\frac{\text{Im}(\nu)}{\text{Re}(\nu)} \right). \quad (1.9)$$

The phase angle is then interpolated to the resolution of the full spectrum and used in equation 1.8 for the phase correction.

Another factor that can cause a departure from the above theory, is the divergence of the beam of radiation as it passes through the spectrometer. The difference in distance, x , travelled by a centrally aligned ray and a ray diverging with angle α as a function of optical path difference is given by

$$x = \frac{2\delta}{\cos \alpha} - 2\delta \quad (1.10)$$

which can be approximated to

$$x = \delta\alpha^2 \quad (1.11)$$

if α is small. As δ increases the central ray and the diverging ray become increasingly out of phase and the contrast between light and dark fringes at the detector decreases until the two rays are completely out of phase and the fringe contrast at the detector disappears completely (Griffiths & de Haseth 1986). This has the effect of limiting the resolution of the interferogram as no further information is added by scanning beyond this limit. Therefore, it is sometimes called self-apodisation. This beam divergence also has the effect of introducing a wavenumber dependent frequency shift in the wavenumber scale recorded by the interferometer due to the different effective path differences seen by the central and extreme rays. Additionally,

many designs of Fourier transform spectrometer contain a meteorology laser which governs the sampling of the interferogram by measuring the position of the scanning mirror. The metrology laser must be slightly offset from the infrared optical path and any misalignment between these two systems can also introduce a wavenumber dependent frequency shift. This shift can be determined by a comparison between the measured spectrum and a reference spectrum, such as one calculated using a radiative transfer code. Once determined the wavenumber shift should remain consistent unless the alignment of the interferometer or the average angle of the beam passing through the interferometer is changed.

Finally, to determine the absolute radiance measured by the spectrometer, the response function of the instrument must be determined. A single measured spectrum $B(\nu)$ can be related to the absolute radiance signal $L(\nu)$ via the equation

$$B(\nu) = R(\nu)L(\nu) + C(\nu), \quad (1.12)$$

where $R(\nu)$ is the instrument response function and $C(\nu)$ is a background offset which can be caused by instrument self-emission or atmospheric emission. Assuming $C(\nu)$ is constant across measurements, the instrument response function can be calculated by differencing two measurements of known radiance. Usually these are a hot blackbody calibration target and a cold or ambient temperature blackbody calibration target. The instrument response function is then calculated using

$$R(\nu) = \frac{B_{HBB}(\nu) - B_{CBB}(\nu)}{L_{HBB}(\nu, T_{HBB}) - L_{CBB}(\nu, T_{CBB})} \quad (1.13)$$

where B_{HBB} and B_{CBB} are the measured signals from the hot and cold blackbodies and L_{HBB} and L_{CBB} are the blackbody radiances from the hot and cold blackbodies at temperatures T_{HBB} and T_{CBB} . This assumes that the blackbodies have a uniform temperature and an emissivity of 1.

By considering equation 1.12, we can find the calibrated scene radiance, L_{scene} , by performing

ing another difference against the measured signal from the hot blackbody calibration target. This cancels out the background offset $C(\nu)$ and means the calibrated scene radiance can be determined using

$$L_{\text{scene}}(\nu) = \frac{B_{\text{scene}}(\nu) - B_{HBB}(\nu)}{I(\nu)} + L_{HBB}(\nu). \quad (1.14)$$

Chapter 2

Developing FINESSE

2.1 Description of FINESSE

The Far INfrarEd Spectrometer for Surface Emissivity (FINESSE) has been developed at Imperial College for the in-situ measurement of surface emissivity. Figure 2.1 shows several photographs of FINESSE. FINESSE consists of a commercial Bruker EM 27 Fourier transform infrared spectrometer (figure 2.1a) coupled with a custom external calibration and scene view system designed and built at Imperial College (figure 2.1b). The spectrometer has a liquid nitrogen cooled extended mercury cadmium telluride (MCT) detector, potassium bromide (KBr) beamsplitter and diamond optical window resulting in a spectral range of 400 to 1600 cm^{-1} (6.3 to 25 μm). The maximum nominal resolution of the spectrometer is 0.5 cm^{-1} corresponding to an optical path difference of 1.21 cm. The external calibration system consists of an ambient temperature and a heated blackbody cavity, hereafter referred to as CBB and HBB respectively, and a gold pointing mirror. The pointing mirror allows the spectrometer to view the blackbody cavities and external scenes at angles ranging from nadir to zenith. The angle of the pointing mirror and the operation of the EM 27 are controlled by a custom graphical user interface which also monitors the temperatures from the calibration targets. These temperatures are measured using platinum resistance thermometers (PRTs) which are logged using an Omega DP9800. Additional PRTs can be added to monitor extra temperatures as required. The EM

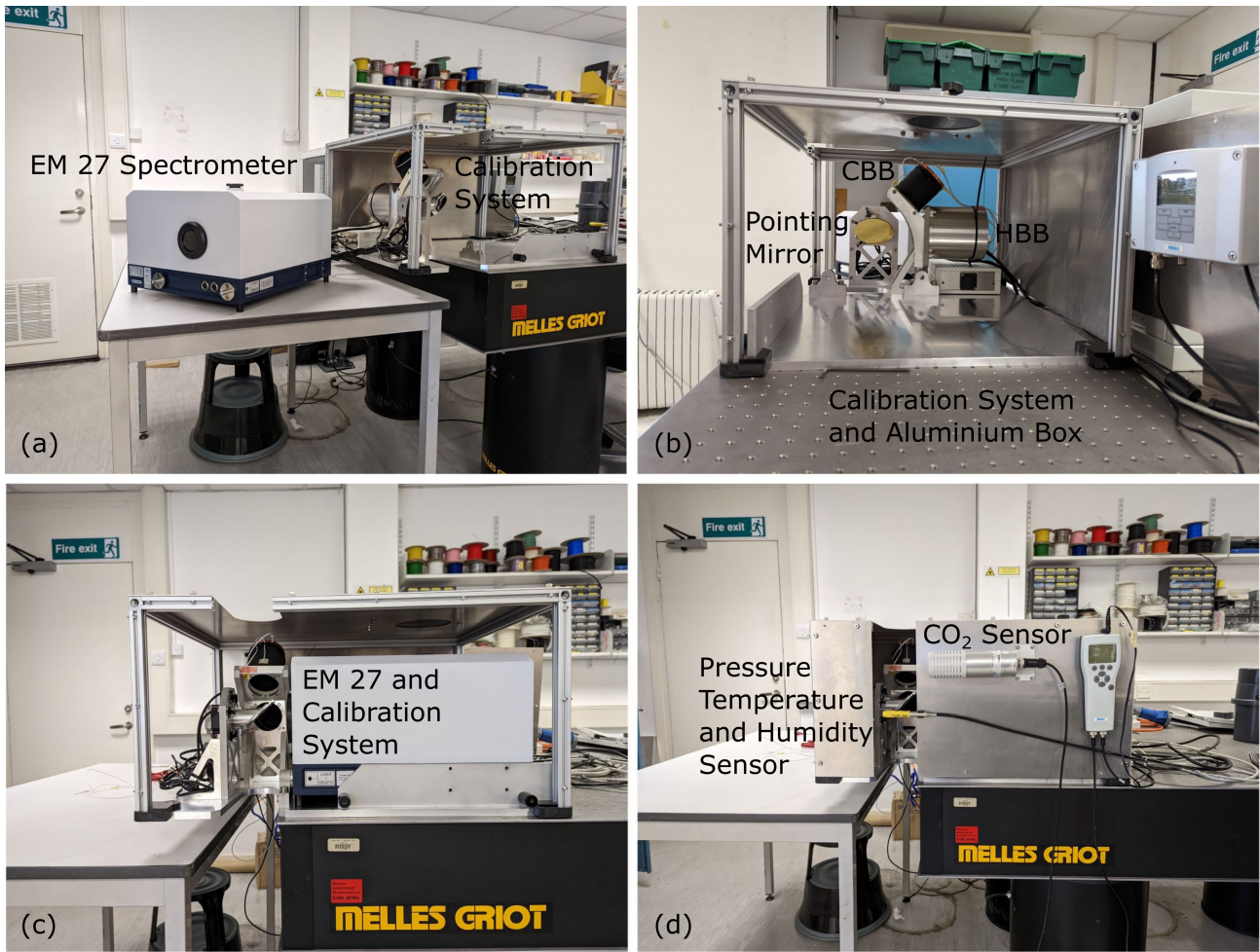


Figure 2.1: Photographs of FINESSE. (a) The Bruker EM 27 and calibration system. (b) Another view of the calibration and pointing system showing the hot black body (HBB) cold black body (CBB) and pointing mirror. (c) The EM 27 in place within the aluminium box. (d) The aluminium box closed up and the CO₂ and temperature, pressure, humidity sensors in place.

27 and calibration system are enclosed in an aluminium box (figure 2.1d). The electronics and controllers for the pointing system and heaters are housed in a separate electronics box. The interferograms measured by the EM 27 are accompanied by additional environmental monitoring. This monitoring consists of pressure, temperature and humidity measurements from a Vaisala PTU300 (PTU) and CO₂ measurements from a Vaisala GMP343. These sensors are mounted on the aluminium box which encases the interferometer(figure 2.1d). When making measurements FINESSE will generally cycle through views of the hot and cold calibration targets and then the scene.

2.2 Calibration process

The most straightforward way to calibrate the spectra produced by FINESSE would be to work in the frequency domain, i.e. with the spectra, using the standard Mertz correction described in section 1.1. However, initial measurements of downwelling radiance showed unexpectedly high radiance in the atmospheric window. Further investigation revealed anomalous behaviour of the phase function similar to that observed by Revercomb et al. (1988) when developing the calibration system for the High-Resolution Interferometer Sounder (Murray personal communication, Revercomb et al. 1988). As Revercomb et al. explain, the standard method only considers the phase component from the sources measured by the interferometer but does not account for radiance from the instrument itself, which can have different phase characteristics. This is particularly important for our purposes as, when measuring cold surfaces such as ice or radiation emanating from high in the atmosphere, the scene radiance may be low compared to the radiance from the instrument. Therefore, to calculate the response function for FINESSE, we have adapted the method described by Revercomb et al.

The response function is calculated by first differencing the measured interferograms for the hot and cold targets

$$Int_{resp} = Int_{HBB} - Int_{CBB}, \quad (2.1)$$

see steps 1 and 2 in figure 2.2.

A complex Fourier transform is then performed on Int_{resp} to produce a complex difference spectrum $\tilde{S}(\nu)$, (fig 2.2 step 3) where

$$\tilde{S}(\nu) = S_{re}(\nu) + iS_{im}(\nu). \quad (2.2)$$

We then perform a phase correction on the complex difference spectrum. The phase function (fig 2.2 step 4) is calculated using equation 1.8 and is then applied to $\tilde{S}(\nu)$ to produce a phase corrected difference spectrum, $\tilde{S}^{corrected}(\nu)$ (fig 2.2 step 5), where

$$\tilde{S}^{corrected}(\nu) = S_{re}^{corrected}(\nu) + iS_{im}^{corrected}(\nu) \quad (2.3)$$

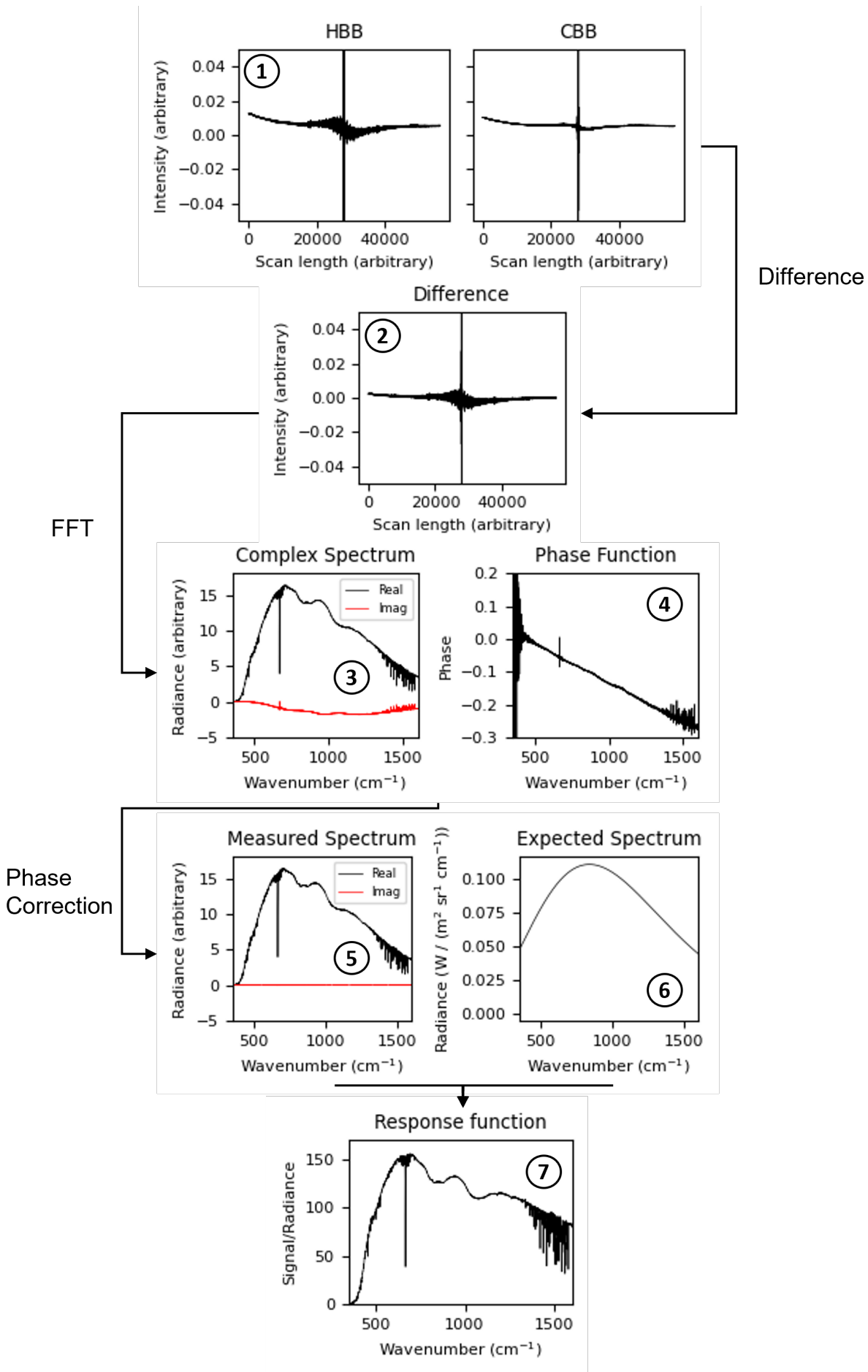


Figure 2.2: A schematic showing how the FINESSE response function is calculated.

The real part of this phase corrected difference spectrum, $S_{re}^{corrected}$ is used to calculate the response function, $I(\nu)$ (fig 2.2 steps 6 and 7),

$$I(\nu) = \frac{S_{re}^{corrected}(\nu)}{[L_{HBB}(\nu, T_{HBB}) - L_{CBB}(\nu, T_{CBB})]} \quad (2.4)$$

where $L_{HBB}(\nu, T_{HBB})$ and $L_{CBB}(\nu, T_{CBB})$ are the wavenumber dependent radiances produced by the HBB and CBB at temperatures, T_{HBB} and T_{CBB} , respectively.

The calibrated scene radiance, $L_{scene}(\nu)$, is found by first differencing the scene and HBB interferograms to produce a difference interferogram, Int_{diff} ,

$$Int_{diff} = Int_{scene} - Int_{HBB}. \quad (2.5)$$

A Fourier transform is applied to this difference interferogram and the resulting spectrum is then phase corrected. This produces a phase corrected but uncalibrated complex scene view spectrum,

$$\tilde{S}^{scene}(\nu) = S_{real}^{scene} + iS_{im}^{scene}. \quad (2.6)$$

Finally, the calibrated scene radiance, $L_{scene}(\nu)$, is calculated using the response function,

$$L_{scene}(\nu) = \frac{S_{real}^{scene}(\nu)}{I(\nu)} + L_{HBB}(\nu, T_{HBB}). \quad (2.7)$$

As mentioned in section 1.1 we must also adjust the wavenumber scale to account for a slight misalignment between the laser and infrared beam and the divergence of the infrared beam. This stretch to the wavenumber scale was determined by the comparison of transmission spectra recorded by the instrument with LBLRTM simulations (Murray, Personal Communication, 2022). The wavenumber multiplier was found to be 1.00016 or 0.016% of the quoted wavenumber scale, which, although small, could be seen at the edges of the sharp water vapour lines.

2.3 Determination of NESR and Calibration Uncertainty

The NESR for the measurements is calculated using the method developed for TAFTS Green (2003). This is done using the imaginary part of $\tilde{S}^{scene}(\nu)$. First this is converted into radiance units using the response function

$$L_{im}(\nu) = \frac{S_{im}^{scene}(\nu)}{I(\nu)}. \quad (2.8)$$

The standard deviation of $L_{im}(\nu)$ is then calculated across a rolling window to produce the NESR as a function of frequency. For FINESSE we use a window size of 20 samples.

The calibration uncertainty is determined by considering the accuracy of the PRTs used to measure the temperatures of the HBB and CBB. This accuracy is 0.2K. To calculate the calibration uncertainty, three versions of the calibrated spectra are produced. The original spectrum is calculated using the measured temperatures of the HBB and CBB. The second spectrum is an upper radiance bound which is calculated using a positive offset of 0.2K to the CBB temperature and a negative offset of 0.2K to the HBB temperature. The third spectrum is as a lower radiance bound calculated using a positive offset to the HBB temperature and a negative offset to the CBB temperature. The difference between the original spectrum and the upper and lower spectra are taken as the upper and lower values of the calibration uncertainty.

Bibliography

Davis, S. P., Abrams, M. C. & Brault, J. W. (2001), *Fourier Transform Spectrometry*, Academic Press, San Diego.

Green, P. (2003), The Development of a Fourier Transform Spectrometer to Measure Far IR Fluxes in the Upper Troposphere, PhD thesis, Imperial College London.

Griffiths, P. R. & de Haseth, J. A. (1986), *Fourier Transform Infrared Spectrometry*, John Wiley & Sons, New York.

Mertz, L. (1965), *Transformations in Optics*, John Wiley & Sons, Inc., New York.

Michelson, A. A. & Morley, E. W. (1887), ‘On the relative motion of the earth and the luminiferous ether’, *American Journal of Science* **s3-34**(203), 333–345.

URL: <https://www.ajsonline.org/content/s3-34/203/333>

Revercomb, H. E., Buijs, H., Howell, H. B., LaPorte, D. D., Smith, W. L. & Sromovsky, L. A. (1988), ‘Radiometric calibration of ir fourier transform spectrometers: solution to a problem with the high-resolution interferometer sounder’, *Appl. Opt.* **27**(15), 3210–3218.